
This copy is for your personal, non-commercial use only.

If you wish to distribute this article to others, you can order high-quality copies for your colleagues, clients, or customers by [clicking here](#).

Permission to republish or repurpose articles or portions of articles can be obtained by following the guidelines [here](#).

The following resources related to this article are available online at www.sciencemag.org (this information is current as of October 19, 2014):

Updated information and services, including high-resolution figures, can be found in the online version of this article at:

<http://www.sciencemag.org/content/276/5309/122.full.html>

This article **cites 15 articles**, 2 of which can be accessed free:

<http://www.sciencemag.org/content/276/5309/122.full.html#ref-list-1>

This article has been **cited by** 100 articles hosted by HighWire Press; see:

<http://www.sciencemag.org/content/276/5309/122.full.html#related-urls>

This article appears in the following **subject collections**:

Ecology

<http://www.sciencemag.org/cgi/collection/ecology>

A General Model for the Origin of Allometric Scaling Laws in Biology

Geoffrey B. West, James H. Brown,* Brian J. Enquist

Allometric scaling relations, including the 3/4 power law for metabolic rates, are characteristic of all organisms and are here derived from a general model that describes how essential materials are transported through space-filling fractal networks of branching tubes. The model assumes that the energy dissipated is minimized and that the terminal tubes do not vary with body size. It provides a complete analysis of scaling relations for mammalian circulatory systems that are in agreement with data. More generally, the model predicts structural and functional properties of vertebrate cardiovascular and respiratory systems, plant vascular systems, insect tracheal tubes, and other distribution networks.

Biological diversity is largely a matter of body size, which varies over 21 orders of magnitude (1). Size affects rates of all biological structures and processes from cellular metabolism to population dynamics (2, 3). The dependence of a biological variable Y on body mass M is typically characterized by an allometric scaling law of the form

$$Y = Y_0 M^b \quad (1)$$

where b is the scaling exponent and Y_0 a constant that is characteristic of the kind of organism. If, as originally thought, these relations reflect geometric constraints, then b should be a simple multiple of one-third. However, most biological phenomena scale as quarter rather than third powers of body mass (2–4): For example, metabolic rates B of entire organisms scale as $M^{3/4}$; rates of cellular metabolism, heartbeat, and maximal population growth scale as $M^{-1/4}$; and times of blood circulation, embryonic growth and development, and life-span scale as $M^{1/4}$. Sizes of biological structures scale similarly: For example, the cross-sectional areas of mammalian aortas and of tree trunks scale as $M^{3/4}$. No general theory explains the origin of these laws. Current hypotheses, such as resistance to elastic buckling in terrestrial organisms (5) or diffusion of materials across hydrodynamic boundary layers in aquatic organisms (6), cannot explain why so many biological processes in nearly all kinds of animals (2, 3), plants (7), and microbes (8) exhibit quarter-power scaling.

We propose that a common mechanism

underlies these laws: Living things are sustained by the transport of materials through linear networks that branch to supply all parts of the organism. We develop a quantitative model that explains the origin and ubiquity of quarter-power scaling; it predicts the essential features of transport systems, such as mammalian blood vessels and bronchial trees, plant vascular systems, and insect tracheal tubes. It is based on three unifying principles or assumptions: First, in order for the network to supply the entire volume of the organism, a space-filling fractal-like branching pattern (9) is required. Second, the final branch of the network (such as the capillary in the circulatory system) is a size-invariant unit (2). And third, the energy required to distribute resources is minimized (10); this final restriction is basically equivalent to minimizing the total hydrodynamic resistance of the system. Scaling laws arise from the interplay between physical and geometric constraints implicit in these three principles. The model presented here should be viewed as an idealized representation in that we ignore complications such as tapering of vessels, turbulence, and nonlinear effects. These play only a minor role in determining the dynamics of the entire network and could be incorporated in more detailed analyses of specific systems.

Most distribution systems can be described by a branching network in which the sizes of tubes regularly decrease (Fig. 1). One version is exhibited by vertebrate circulatory and respiratory systems, another by the "vessel-bundle" structure of multiple parallel tubes, characteristic of plant vascular systems (11). Biological networks vary in the properties of the tube (elastic to rigid), the fluid transported (liquid to gas), and the nature of the pump (a pulsatile compression pump in the cardiovascular system, a pulsatile bellows pump in the respiratory system, diffusion in insect

- p888, which contains a Bam HI to Not I fragment encoding a full-length profilin cDNA (16); p889, which encodes a mutant form of profilin, Pfy1p-3, lacking the last three amino acids (18); p890, which contains the Bgl II to Stu I fragment from p182 (26), encoding Bni1p(1227–1397); p813, which contains the Bgl II to Not I fragment from p182, encoding Bni1p(1414–1953); and p951, which contains the Hpa I to Not I fragment from p182, encoding Bni1p(1647–1953). The pJG4-5–derived plasmids were p561, which contains the Bam HI to Not I fragment from p532 (26), encoding Bni1p(1–1953); p717, which contains the Bam HI to Eco47 III fragment from p532, encoding Bni1p(1–1214); p558, which contains the Eco 47III to Not I fragment from p182, encoding Bni1p(1215–1953); p913, which contains the Bgl II to Stu I fragment from p182, encoding Bni1p(1227–1397); p929, which contains the Bgl II to Not I fragment from p182, encoding Bni1p(1414–1953); p952, which contains the Hpa I to Not I fragment from p182, encoding Bni1p(1647–1953); and p887, which contains the Bam HI to Not I fragment encoding a full-length profilin cDNA (16). The pACT-derived plasmid was p1124, encoding full-length Act1p as isolated in a catch and release screen (22). The pGAD-C–derived plasmid was p688, encoding the COOH-terminal 311 amino acids (478–788) of Bud6p, as isolated in a catch and release screen (22).
29. For localization of Bni1p, SY2625 (11) cells carrying a multicopy plasmid encoding either HA-tagged Bni1p [pY39tet1 (9)] or nontagged Bni1p were induced to form mating projections (12). HA-Bni1p was localized by immunofluorescence with monoclonal antibody HA.11 (Berkeley Antibody Company) as described [J. R. Pringle, A. E. M. Adams, D. G. Drubin, B. K. Haarer, *Methods Enzymol.* **194**, 565 (1991)]. For localization of Bud6p, SY2625 cells expressing GFP-Bud6p (23) or containing the control plasmid pRS316 (26) were induced to form mating projections (12), then observed by fluorescence microscopy with the use of a fluorescein isothiocyanate filter set.
30. Yeast cells of strain B5459 (*MATa pep4::HIS3 prb1Δ1-6R ura3 trp1 lys2 leu2 his3Δ200 can1*) carrying p1025 (26) were grown to mid-log phase in raffinose medium, and galactose was added to induce the production of HA-tagged Bni1p(1215–1953). After 1 hour, extracts were prepared by grinding cells with glass beads in lysis buffer [0.6 M sorbitol, bovine serum albumin (1%), 140 mM NaCl, 5 mM EDTA, 50 mM tris-HCl (pH 7.6), 0.06% Triton X-100, 2 mM phenylmethylsulfonyl fluoride, aprotinin (10 μg/ml)] as described (2). *Escherichia coli* strain BL 21 (Novagen) was transformed with pGEX-3X (Pharmacia) or p907 (26) and induced for expression of GST or GST-profilin, respectively. GST proteins were purified on glutathione-Sepharose (Pharmacia) and washed twice with phosphate-buffered saline (PBS) [140 mM NaCl, 2.7 mM KCl, 10 mM Na₂HPO₄, 1.8 mM KH₂PO₄ (pH 7.3)]. Glutathione-Sepharose beads with GST or GST-profilin bound were then added to the yeast extract containing HA-Bni1p(1215–1953) and incubated on ice. After 45 min, the beads were collected and washed twice with PBS. The GST proteins and associated proteins were eluted with glutathione [10 mM glutathione, 50 mM tris-HCl (pH 8.0)] and subjected to immunoblot analysis with antibodies to GST (Pharmacia) or the HA epitope (29) as described (27).
31. We thank D. Amberg, B. Andrews, R. Brent, R. Dorer, S. J. Elledge, S. Givan, B. K. Haarer, J. Horecka, P. James, I. Sadowski, M. Tyers, and J. Zahner for plasmids and yeast strains; B. Brandhorst, J. Brown, N. Davis, S. Kim, B. Nelson, and I. Pot for comments on the manuscript; and G. Poje and I. Pot for assistance with experiments. Supported by grants to C.B. from the Natural Sciences and Engineering Research Council of Canada and the National Cancer Institute of Canada; by a grant from the Swiss National Science Foundation to M.P.; and by NIH grant GM31006 to J.R.P.

G. B. West, Theoretical Division, T-8, Mail Stop B285, Los Alamos National Laboratory, Los Alamos, NM 87545, and The Santa Fe Institute, 1399 Hyde Park Road, Santa Fe, NM 87501, USA.

J. H. Brown and B. J. Enquist, Department of Biology, University of New Mexico, Albuquerque, NM 87131, and The Santa Fe Institute, 1399 Hyde Park Road, Santa Fe, NM 87501, USA.

*To whom correspondence should be addressed. E-mail: jhbrown@unm.edu

2 December 1996; accepted 10 February 1997

tracheae, and osmotic and vapor pressure in the plant vascular system). In spite of these differences, these networks exhibit essentially the same scaling laws.

For convenience we shall use the language of the cardiovascular system, namely, aorta, arteries, arterioles, and capillaries; the correspondence to other systems is straightforward. In the general case, the network is composed of N branchings from the aorta (level 0) to the capillaries (level N , denoted here by a subscript c) (Fig. 1C). A typical branch at some intermediate level k has length l_k , radius r_k , and pressure drop Δp_k (Fig. 1D). The volume rate of flow is $\dot{Q}_k = \pi r_k^2 \bar{u}_k$ where \bar{u}_k is the flow velocity averaged over the cross section and, if necessary, over time. Each tube branches into n_k smaller ones (12), so the total number of branches at level k is $N_k = n_0 n_1 \dots n_k$. Because fluid is conserved as it flows through the system

$$\dot{Q}_0 = N_k \dot{Q}_k = N_k \pi r_k^2 \bar{u}_k = N_c \pi r_c^2 \bar{u}_c \quad (2)$$

which holds for any level k . We next introduce the important assumption, the second above, that the terminal units (capillaries) are invariant, so r_c , l_c , \bar{u}_c , and, consequently, Δp_c are independent of body size. Because the fluid transports oxygen and nutrients for metabolism, $\dot{Q}_0 \propto B$; thus, if $B \propto M^a$ (where a will later be determined to be $3/4$), then $\dot{Q}_0 \propto M^a$. Equation 2 therefore predicts that the total number of capillaries must scale as B , that is, $N_c \propto M^a$.

To characterize the branching, we introduce scale factors $\beta_k \equiv r_{k+1}/r_k$ and $\gamma_k \equiv l_{k+1}/l_k$. We shall prove that in order to minimize the energy dissipated in the system in the sense of the third principle above, the network must be a conventional self-similar fractal in that $\beta_k = \beta$, $\gamma_k = \gamma$, and $n_k = n$, all independent of k (an important exception is β_k in pulsatile systems). For a self-similar fractal, the number of branches increases in geometric proportion ($N_k = n^k$) as their size geometrically decreases from level 0 to level N . Before proving self-similarity, we first examine some of its consequences.

Because $N_c = n^N$, the number of generations of branches scales only logarithmically with size

$$N = \frac{a \ln(M/M_0)}{\ln n} \quad (3)$$

where M_0 is a normalization scale for M (13). Thus, a whale is 10^7 times heavier than a mouse but has only about 70% more branchings from aorta to capillary. The total volume of fluid in the network ("blood" volume V_b) is

$$V_b = \sum_{k=0}^N N_k V_k = \sum_{k=0}^N \pi r_k^2 l_k n^k$$

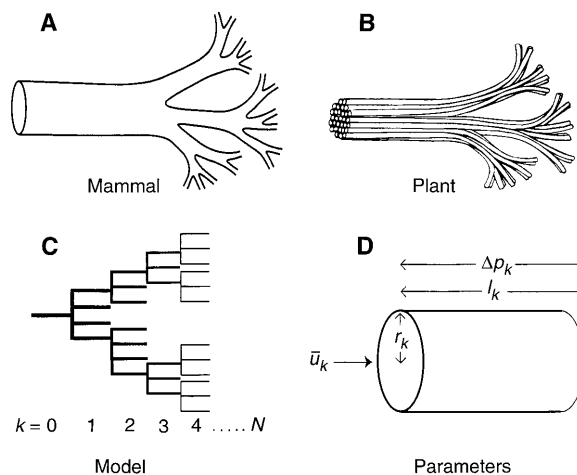


Fig. 1. Diagrammatic examples of segments of biological distribution networks: (A) mammalian circulatory and respiratory systems composed of branching tubes; (B) plant vessel-bundle vascular system composed of diverging vessel elements; (C) topological representation of such networks, where k specifies the order of the level, beginning with the aorta ($k = 0$) and ending with the capillary ($k = N$); and (D) parameters of a typical tube at the k th level.

$$= \frac{(n\gamma\beta^2)^{-(N+1)} - 1}{(n\gamma\beta^2)^{-1} - 1} n^N V_c \quad (4)$$

where the last expression reflects the fractal nature of the system. As shown below, one can also prove from the energy minimization principle that $V_b \propto M$. Because $n\gamma\beta^2 < 1$ and $N \gg 1$, a good approximation to Eq. 4 is $V_b = V_0/(1 - n\gamma\beta^2) = V_c(\gamma\beta^2)^{-N}/(1 - n\gamma\beta^2)$. From our assumption that capillaries are invariant units, it therefore follows that $(\gamma\beta^2)^{-N} \propto M$. Using this relation in Eq. 3 then gives

$$a = -\frac{\ln n}{\ln(\gamma\beta^2)} \quad (5)$$

To make further progress requires knowledge of γ and β . We shall show how the former follows from the space-filling fractal requirement, and the latter, from the energy minimization principle.

A space-filling fractal is a natural structure for ensuring that all cells are serviced by capillaries. The network must branch so that a group of cells, referred to here as a "service volume," is supplied by each capillary. Because $r_k \ll l_k$ and the total number of branchings N is large, the volume supplied by the total network can be approximated by the sum of spheres whose diameters are that of a typical k th-level vessel, namely $4/3\pi(l_k/2)^3 N_k$. For large N , this estimate does not depend significantly on the specific level, although it is most accurate for large k . This condition, that the fractal be volume-preserving from one generation to the next, can therefore be expressed as $4/3\pi(l_k/2)^3 N_k \approx 4/3\pi(l_{k+1}/2)^3 N_{k+1}$. This relation gives $\gamma^3 \beta^3 \equiv (l_{k+1}/l_k)^3 \approx N_k/N_{k+1} = 1/n$, showing that $\gamma_k \approx n^{-1/3} \approx \gamma$ must be independent of k . This result for γ_k is a general property of all space-filling fractal systems that we consider.

The $3/4$ power law arises in the simple case of the classic rigid-pipe model, where the branching is assumed to be area-pre-

serving, that is, the sum of the cross-sectional areas of the daughter branches equals that of the parent, so $\pi r_k^2 = n\pi r_{k+1}^2$. Thus, $\beta_k \equiv r_{k+1}/r_k = n^{-1/2} = \beta$, independent of k . When the area-preserving branching relation, $\beta = n^{-1/2}$, is combined with the space-filling result for γ , Eq. 5 yields $a = 3/4$, so $B \propto M^{3/4}$. Many other scaling laws follow. For example, for the aorta, $r_0 = \beta^{-N} r_c = N_c^{1/2} r_c$ and $l_0 = \gamma^{-N} l_c = N_c^{1/3} l_c$, yielding $r_0 \propto M^{3/8}$ and $l_0 \propto M^{1/4}$. This derivation of the $a = 3/4$ law is essentially a geometric one, strictly applying only to systems that exhibit area-preserving branching. This property has the further consequence, which follows from Eq. 2, that the fluid velocity must remain constant throughout the network and be independent of size. These features are a natural consequence of the idealized vessel-bundle structure of plant vascular systems (Fig. 1B), in which area-preserving branching arises automatically because each branch is assumed to be a bundle of n^{N-k} elementary vessels of the same radius (11). Pulsatile mammalian vascular systems, on the other hand, do not conform to this structure, so for them, we must look elsewhere for the origin of quarter-power scaling laws.

Some features of the simple pipe model remain valid for all networks: (i) The quantities γ and β play a dual scaling role: they determine not only how quantities scale from level 0 (aorta) to N (capillary) within a single organism of fixed size, but also how a given quantity scales when organisms of different masses are compared. (ii) The fractal nature of the entire system as expressed, for example, in the summation in Eq. 4 leads to a scaling different from that for a single tube, given by an individual term in the series. These network systems must therefore be treated as a complete integrated unit; they cannot realistically be modeled by a single or a few representative vessels. (iii) The scaling with M does not

depend on the branching ratio n .

We next consider the dynamics of the network and examine the consequences of the energy minimization principle, which is particularly relevant to mammalian vascular systems. Pulsatile flow, which dominates the larger vessels (aorta and major arteries), must have area-preserving branching, so that $\beta = n^{-1/2}$, leading to quarter-power scaling. The smaller vessels, on the other hand, have the classic "cubic-law" branching (10), where $\beta = n^{-1/3}$, and play a relatively minor role in allometric scaling.

First consider the simpler problem of nonpulsatile flow. For steady laminar flow of a Newtonian fluid, the viscous resistance of a single tube is given by the well-known Poiseuille formula $R_k = 8\mu l_k / \pi r_k^4$, where μ is the viscosity of the fluid. Ignoring small effects such as turbulence and nonlinearities at junctions, the resistance of the entire network is given by (14)

$$Z = \sum_{k=0}^N \frac{R_k}{N_k} = \sum_{k=0}^N \frac{8\mu l_k}{\pi r_k^4 n^k} = \frac{[1 - (n\beta^4/\gamma)^{N+1}]R_c}{(1 - n\beta^4/\gamma)n^N} \quad (6)$$

Now, $n\beta^4/\gamma < 1$ and $N \gg 1$, so a good approximation is $Z = R_c / (1 - n\beta^4/\gamma)N_c$. Because R_c is invariant, $Z \propto N_c^{-1} \propto M^{-a}$, which leads to two important scaling laws: blood pressure $\Delta p = \dot{Q}_0 Z$ must be independent of body size and the power dissipated in the system (cardiac output) $W = \dot{Q}_0 \Delta p \propto M^a$, so that the power expended by the heart in overcoming viscous forces is a size-independent fraction of the metabolic rate. Neither of these results depends on detailed knowledge of n , β , or γ , in contrast to results based on $V_b \propto M$, such as Eq. 5, $a = 3/4$, and $r_0 \propto M^{3/8}$. From Eq. 2, $\dot{Q}_0 = \pi r_0^2 \bar{u}_0$, which correctly predicts that the velocity of blood in the aorta $\bar{u}_0 \propto M^0$ (2). However, an area-preserving scaling relation $\beta = n^{-1/2}$ also implies by means of Eq. 2 that $\bar{u}_k = \bar{u}_0$ for all k . This relation is valid for fluid flow in plant vessels (because of the vascular bundle structure) (11, 15) and insect tracheae (because gas is driven by diffusion) (16); both therefore exhibit area-preserving branching, which leads to $3/4$ power scaling of metabolic rate. Branching cannot be entirely area-preserving in mammalian circulatory systems because blood must slow down to allow materials to diffuse across capillary walls. However, the pulsatile nature of the mammalian cardiovascular system solves the problem.

Energy minimization constrains the network for the simpler nonpulsatile systems. Consider cardiac output as a function of all relevant variables: $W(r_k, l_k, n_k, M)$. To sustain a given metabolic rate in an organism of fixed mass M with a given volume of

blood $V_b(r_k, l_k, n_k, M)$, the minimization principle requires that the cardiac output be minimized subject to a space-filling geometry. To enforce such a constraint, we use the standard method of Lagrange multipliers (λ , λ_k , and λ_M) and so need to minimize the auxiliary function

$$F(r_k, l_k, n) = W(r_k, l_k, n_k, M) + \lambda V_b(r_k, l_k, n_k, M) + \sum_{k=0}^N \lambda_k N_k l_k^3 + \lambda_M M \quad (7)$$

Because $B \propto Q_0$ and $W = \dot{Q}_0^2 Z$, this problem is tantamount to minimizing the impedance Z , which can therefore be used in Eq. 7 in place of W . First, consider the case where $n_k = n$, so that we can use Eqs. 4 and 6 for V_b and Z , respectively. For a fixed mass M , the auxiliary Lagrange function F , which incorporates the constraints, must be minimized with respect to all variables for the entire system (r_k , l_k , and n). This requires $\partial F / \partial l_k = \partial F / \partial r_k = \partial F / \partial n = 0$, which straightforwardly leads to $\beta_k = n^{-1/3}$. More generally, by considering variations with respect to n_k , one can show that $n_k = n$, independent of k . The result, $\beta_k = n^{-1/3}$, is a generalization of Murray's finding (17), derived for a single branching, to the complete network. Now varying M and minimizing F in Eq. 7 ($\partial F / \partial M = 0$) leads to $V_b \propto M$, which is just the relation needed to derive Eq. 5. Although the result $\beta_k = n^{-1/3}$ is independent of k , it is not area-preserving and therefore does not give $a = 3/4$ when used in Eq. 5; instead, it gives $a = 1$. It does, however, solve the problem of slowing blood in the capillaries: Eq. 2 gives $\bar{u}_k / \bar{u}_0 = (n\beta^2)^{-N} = N_c^{-1/3}$. For humans, $N_c \approx 10^{10}$, so $\bar{u}_k / \bar{u}_0 \approx 10^{-3}$, in reasonable agreement with data (18). On the other hand, it leads to an incorrect scaling law for this ratio: $\bar{u}_k / \bar{u}_0 \propto M^{-1/4}$. Incorporating pulsatile flow not only solves these problems, giving the correct scaling relations ($a = 3/4$ and $\bar{u}_k / \bar{u}_0 \propto M^0$), but also gives the correct value for \bar{u}_c / \bar{u}_0 .

A complete treatment of pulsatile flow is complicated; here, we present a simplified version that contains the essential features needed for the scaling problem. When an oscillatory pressure p of angular frequency ω is applied to an elastic (characterized by modulus E) vessel with wall thickness h , a damped traveling wave is created: $p = p_0 e^{i(\omega t - 2\pi z/\lambda)}$. Here, t is time, z is the distance along the tube, λ is the wavelength, and p_0 is the amplitude averaged over the radius; the wave velocity $c = 2\pi\omega\lambda$. Both the impedance Z and the dispersion relation that determines c are derived by solving the Navier-Stokes equation for the fluid coupled to the Navier equations for the vessel wall (19).

In the linearized incompressible-fluid, thin-wall approximation, this problem can be solved analytically to give

$$\left(\frac{c}{c_0}\right)^2 \approx -\frac{J_2(i^{3/2}\alpha)}{J_0(i^{3/2}\alpha)} \quad \text{and} \quad Z \approx \frac{c_0^2 \rho}{\pi r^2 c} \quad (8)$$

Here $\alpha = (\omega\rho/\mu)^{1/2}r$ is the dimensionless Womersley number (13), and $c_0 \equiv (Eh/2\rho r)^{1/2}$ is the Korteweg-Moens velocity. In general, both c and Z are complex functions of ω , so the wave is attenuated and disperses as it propagates. Consider the consequences of these formulas as the blood flows through progressively smaller tubes: For large tubes, α is large (in a typical human artery, $\alpha \approx 5$), and viscosity plays almost no role. Equation 8 then gives $c = c_0$ and $Z = \rho c_0 / \pi r^2$; because both of these are real quantities, the wave is neither attenuated nor dispersed. The r dependence of Z has changed from the nonpulsatile r^{-4} behavior to r^{-2} . Minimizing energy loss now gives h_k/r_k (and, therefore, c_k) independent of k and, most importantly, an area-preserving law at the junctions, so $\beta_k = n^{-1/2}$. This relation ensures that energy-carrying waves are not reflected back up the tubes at branch points and is the exact analog of impedance matching at the junctions of electrical transmission lines (18). As k increases, the sizes of tubes decrease, so $\alpha \rightarrow 0$ (in human arterioles, for example, $\alpha \approx 0.05$), and the role of viscosity increases, eventually dominating the flow. Equation 8 then gives $c \approx i^{1/2}\alpha c_0/4 \rightarrow 0$, in agreement with observation (18). Because c and, consequently, λ now have imaginary parts, the traveling wave is heavily damped, leaving an almost steady oscillatory flow whose impedance is, from Eq. 8, given by the Poiseuille formula; that is, the r^{-4} behavior is restored. Thus, for large k , corresponding to small vessels, $\beta_k = n^{-1/3}$. We conclude that for pulsatile flow, β_k is not independent of k but rather has a steplike behavior (Fig. 2). This picture

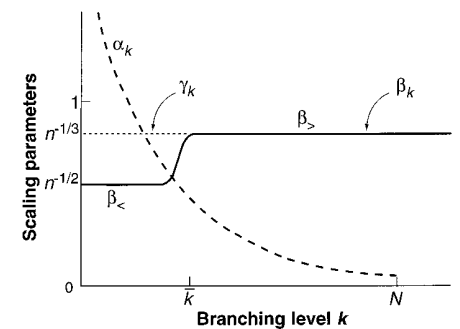


Fig. 2. Schematic variation of the Womersley number α_k and the scaling parameters β_k and γ_k with level number (k) for pulsatile systems. Note the steplike change in β_k at $k = \bar{k}$ from area-preserving pulse-wave flow in major vessels to area-increasing Poiseuille-type flow in small vessels.

is well supported by empirical data (18, 20, 21). The crossover from one behavior to the other occurs over the region where the wave and Poiseuille impedances are comparable in size. The approximate value of k where this occurs (say, \bar{k}) is given by $r_0^2/l_{\bar{k}} \approx 8\mu/\rho c_0$, leading to $N - \bar{k} \equiv \bar{N} \approx \ln(8\mu l_c/\rho c_0 r_c^2)/\ln n$, independent of M . Thus, the number of generations where Poiseuille flow dominates should be independent of body size. On the other hand, the crossover point itself grows logarithmically: $\bar{k} \propto N \propto \ln M$. For humans, with $n = 3$ (21), $\bar{N} \approx 15$ and $N \approx 22$ (assuming $N_c \approx 2 \times 10^{10}$), whereas with $n = 2$, $\bar{N} \approx 24$ and $N \approx 34$. These values mean that in humans Poiseuille flow begins to compete with the pulse wave after just a few branchings, dominating after about seven. In a 3-g shrew, Poiseuille flow begins to dominate shortly beyond the aorta.

The derivation of scaling laws based on β_k derived from Eqs. 7 and 8 (Fig. 2) leads to the same results as before. For simplicity, assume that the crossover is sharp; using a gradual transition does not change the resulting scaling laws. So, for $k > \bar{k}$, define $\beta_k \equiv \beta_{>} = n^{-1/3}$ and, for $k < \bar{k}$, $\beta_k \equiv \beta_{<} = n^{-1/2}$. This predicts that area preservation only persists in the pulsatile region from the aorta through the large arteries, at most until $k \approx \bar{k}$. First consider the radius of the aorta r_0 : its scaling behavior is now given by $r_0 \equiv r_c \beta_{>}^{-N} \beta_{<}^{-\bar{k}} = r_c n^{1/3N+1/6\bar{k}} = r_c n^{1/2N-1/6N}$, which gives $r_0 \propto M^{3/8}$ and, for humans, $r_0/r_c \approx 10^4$, in agreement with data (2). Using Eq. 3 we obtain, for the ratio of fluid velocity in the aorta to that in the capillary, $\bar{u}_0/\bar{u}_c = N_c(r_c/r_0)^2 = n^{\bar{N}/3}\bar{u}_0/\bar{u}_c \approx 250$, independent of M , again in agreement with data. Because γ reflects the

space-filling geometry, it remains unchanged, so we still have $l_0 \propto M^{1/4}$. Blood volume V_b , however, is more complicated

$$V_b = \frac{V_c}{(\beta_{>}^2 \gamma)^N} \left\{ \left(\frac{\beta_{>}}{\beta_{<}} \right)^{2\bar{k}} \frac{1 - (n\beta_{<}^2 \gamma)^{\bar{k}}}{1 - (n\beta_{<}^2 \gamma)} + \left[\frac{1 - (n\beta_{>}^2 \gamma)^N}{1 - (n\beta_{>}^2 \gamma)} - \frac{1 - (n\beta_{<}^2 \gamma)^{\bar{k}}}{1 - (n\beta_{<}^2 \gamma)} \right] \right\} \quad (9)$$

This formula is a generalization of Eq. 4 and is dominated by the first term, which represents the contribution of the large tubes (aorta and arteries). Thus, $V_b \propto n^{N+1/3\bar{k}} \propto n^{4/3}N$, which, because it must scale as M , leads, as before, to $a = 3/4$. As size decreases, the second term, representing the cubic branching of small vessels, becomes increasingly important. This behavior predicts small deviations from quarter-power scaling ($a \gtrsim 3/4$), observed in the smallest mammals (2). An expression analogous to Eq. 9 can be derived for the total impedance of the system Z . It is dominated by the small vessels (arterioles and capillaries) and, as before, gives Δp and $\bar{u}_0 \propto M^0$.

In order to understand allometric scaling, it is necessary to formulate an integrated model for the entire system. The present model should be viewed as an idealized zeroth-order approximation: it accounts for many of the features of distribution networks and can be used as a point of departure for more detailed analyses and models. In addition, because it is quantitative, the coefficients, Y_0 of Eq. 1, can also, in principle, be derived. It accurately predicts the known scaling relations of the mammalian

cardiovascular system (Table 1); data are needed to test other predictions. For example, the invariance of capillary parameters implies $N_c \propto M^{3/4}$ rather than the naive expectation $N_c \propto M$, so the volume serviced by each capillary must scale as $M^{1/4}$, and capillary density per cross-sectional area of tissue, as $M^{-1/12}$.

A minor variant of the model describes the mammalian respiratory system. Although pulse waves are irrelevant because the tubes are not elastic, the formula for Z is quite similar to Eq. 8. The fractal bronchial tree terminates in $N_A \propto M^{3/4}$ alveoli. The network is space-filling, and the alveoli play the role of the service volume accounting for most of the total volume of the lung, which scales as M . Thus, the volume of an alveolus $V_A \propto M^{1/4}$, its radius $r_A \propto M^{1/12}$, and its surface area $A_A \propto r_A^2 \propto M^{1/6}$, so the total surface area of the lung $A_L = N_A A_A \propto M^{11/12}$. This explains the paradox (22) that A_A scales with an exponent closer to 1 than the $3/4$ seemingly needed to supply oxygen. The rate of oxygen diffusion across an alveolus, which must be independent of M , is proportional to $\Delta p_{O_2} A_A / r_A$. Thus, $\Delta p_{O_2} \propto M^{-1/12}$, which must be compensated for by a similar scaling of the oxygen affinity of hemoglobin. Available data support these predictions (Table 1).

Our model provides a theoretical, mechanistic basis for understanding the central role of body size in all aspects of biology. Considering the many functionally interconnected parts of the organism that must obey the constraints, it is not surprising that the diversity of living and fossil organisms is based on the elaboration of a few successful designs. Given the need to redesign the entire system whenever body size changes,

Table 1. Values of allometric exponents for variables of the mammalian cardiovascular and respiratory systems predicted by the model compared

with empirical observations. Observed values of exponents are taken from (2, 3); ND denotes that no data are available.

Cardiovascular			Respiratory		
Variable	Exponent		Variable	Exponent	
	Predicted	Observed		Predicted	Observed
Aorta radius r_0	$3/8 = 0.375$	0.36	Tracheal radius	$3/8 = 0.375$	0.39
Aorta pressure Δp_0	$0 = 0.00$	0.032	Interpleural pressure	$0 = 0.00$	0.004
Aorta blood velocity u_0	$0 = 0.00$	0.07	Air velocity in trachea	$0 = 0.00$	0.02
Blood volume V_b	$1 = 1.00$	1.00	Lung volume	$1 = 1.00$	1.05
Circulation time	$1/4 = 0.25$	0.25	Volume flow to lung	$3/4 = 0.75$	0.80
Circulation distance l	$1/4 = 0.25$	ND	Volume of alveolus V_A	$1/4 = 0.25$	ND
Cardiac stroke volume	$1 = 1.00$	1.03	Tidal volume	$1 = 1.00$	1.041
Cardiac frequency ω	$-1/4 = -0.25$	-0.25	Respiratory frequency	$-1/4 = -0.25$	-0.26
Cardiac output \dot{E}	$3/4 = 0.75$	0.74	Power dissipated	$3/4 = 0.75$	0.78
Number of capillaries N_c	$3/4 = 0.75$	ND	Number of alveoli N_A	$3/4 = 0.75$	ND
Service volume radius	$1/12 = 0.083$	ND	Radius of alveolus r_A	$1/12 = 0.083$	0.13
Womersley number α	$1/4 = 0.25$	0.25	Area of alveolus A_A	$1/6 = 0.083$	ND
Density of capillaries	$-1/12 = -0.083$	-0.095	Area of lung A_L	$11/12 = 0.92$	0.95
O_2 affinity of blood P_{50}	$-1/12 = -0.083$	-0.089	O_2 diffusing capacity	$1 = 1.00$	0.99
Total resistance Z	$-3/4 = -0.75$	-0.76	Total resistance	$-3/4 = -0.75$	-0.70
Metabolic rate B	$3/4 = 0.75$	0.75	O_2 consumption rate	$3/4 = 0.75$	0.76

either during ontogeny or phylogenetic diversification, small deviations from quarter-power scaling sometimes occur (3, 23). However, when body sizes vary over many orders of magnitude, these scaling laws are obeyed with remarkable precision. Moreover, the predicted scaling properties do not depend on most details of system design, including the exact branching pattern, provided it has a fractal structure (24). Significantly, nonfractal systems, such as combustion engines and electric motors, exhibit geometric (third-power) rather than quarter-power scaling (1). Because the fractal network must still fill the entire D -dimensional volume, our result generalizes to $a = D/(D + 1)$. Organisms are three-dimensional, which explains the 3 in the numerator of the $3/4$ power law, but it would be instructive to examine nearly two-dimensional organisms such as bryozoans and flatworms. The model can potentially explain how fundamental constraints at the level of individual organisms lead to corresponding quarter-power allometries at other levels. The constraints of body size on the rates at which resources can be taken up from the environment and transported and transformed within the body ramify to cause quarter-power scaling in such diverse phenomena as rate and duration of embryonic and postembryonic growth and development, interval between clutches, age of first reproduction, life span, home range and territory size, population density, and maximal population growth rate (1–3). Because organisms of different body sizes have different requirements for resources and operate on different spatial and temporal scales, quarter-power allometric scaling is perhaps the single most pervasive theme underlying all biological diversity.

REFERENCES AND NOTES

1. T. A. McMahon and J. T. Bonner, *On Size and Life* (Scientific American Library, New York, 1983); J. T. Bonner, *The Evolution of Complexity by Means of Natural Selection* (Princeton Univ. Press, Princeton, NJ, 1983); J. H. Brown, *Macroecology* (Univ. of Chicago Press, Chicago, 1995).
2. K. Schmidt-Nielsen, *Scaling: Why Is Animal Size so Important?* (Cambridge Univ. Press, Cambridge, 1984); W. A. Calder III, *Size, Function and Life History* (Harvard Univ. Press, Cambridge, MA, 1984).
3. R. H. Peters, *The Ecological Implications of Body Size* (Cambridge Univ. Press, Cambridge, 1983).
4. H. A. Feldman and T. A. McMahon, *Respir. Physiol.* **52**, 149 (1983).
5. T. A. McMahon, *Science* **179**, 1201 (1973).
6. M. R. Patterson, *ibid.* **255**, 1421 (1992).
7. K. J. Niklas, *Plant Allometry: The Scaling of Form and Process* (Univ. of Chicago Press, Chicago, 1994); *Am. J. Bot.* **81**, 134 (1994).
8. A. M. Hemmingsen, *Rep. Steno Mem. Hosp. (Copenhagen)* **4**, 1 (1950); *ibid.* **9**, 1 (1960).
9. B. B. Mandelbrot, *The Fractal Geometry of Nature* (Freeman, New York, 1977).
10. D'A. W. Thompson, *On Growth and Form* (Cambridge Univ. Press, Cambridge, 1942).
11. K. Shinozaki *et al.*, *Jpn. J. Ecol.* **14**, 97 (1964); *ibid.*,

- p. 133; see also M. H. Zimmerman, *Xylem Structure and the Ascent of Sap* (Springer-Verlag, Berlin, 1983); M. T. Tyree and F. W. Ewers, *New Phytol.* **119**, 345 (1991).
12. The branching of a vessel at level k into n_k smaller vessels (Fig. 1) is assumed to occur over some small, but finite, distance that is much smaller than either l_k or l_{k+1} . This relation is similar to that assumed in the Strahler method [A. N. Strahler, *Trans. Am. Geophys. Union* **34**, 345 (1953); (11, 21)]. A generalization to nonuniform branching, where the radii and lengths at a given level may vary, is straightforward.
 13. Normalization factors, such as M_0 , will generally be suppressed, as in Eq. 1. In general, all quantities should be expressed in dimensionless form; note, however, that this does not guarantee that they are size independent and scale as M^0 . For example, the Womersley number, α of Eq. 8, although dimensionless, scales as $M^{1/4}$.
 14. This formula is not valid for plant vessel bundles because plants are composed of multiple parallel vessel elements. Their resistance is given by $Z = 8\mu l / N_k \pi r_c^4$, where l is the length of a single vessel element, r_c is its radius, and N_k is their total number.
 15. This relation holds for plant vessels from the roots to the leaves, but not within leaves [M. J. Canney, *Philos. Trans. R. Soc. London Ser. B* **341**, 87 (1993)].
 16. A. Krogh, *Pluegers Arch. Gesamte Physiol. Menschen Tiere* **179**, 95 (1920).
 17. C. D. Murray, *Proc. Natl. Acad. Sci. U.S.A.* **12**, 207 (1926).
 18. C. G. Caro *et al.*, *The Mechanics of Circulation* (Oxford Univ. Press, Oxford, 1978).
 19. J. R. Womersley, *Philos. Mag.* **46**, 199 (1955); *J. Physiol. (London)* **127**, 553 (1955).
 20. See, for example, A. S. Ilerall, *Math. Biosci.* **1**, 375 (1967) and T. F. Sherman, *J. Gen. Physiol.* **78**, 431 (1981), which contain summaries of earlier data; also M. Zamir *et al.*, *J. Biomech.* **25**, 1303 (1992) and J. K.-J. Li, *Comparative Cardiovascular Dynamics of*

Mammals (CRC Press, Boca Raton, FL, 1996). Care must be taken in comparing measurements with prediction, particularly if averages over many successive levels are used. For example, if $A_k = \sum_k \pi r_k^2$ is the total cross-sectional area at level k , then for the aorta and major arteries, where $k < k$ and the branching is area-preserving, we predict $A_0 = A_k$. Suppose, however, that the first K levels are grouped together. Then, if the resulting measurement gives \bar{A}_K , area-preserving predicts $\bar{A}_K = KA_0$ (but not $\bar{A}_K = A_0$). It also predicts $r_0^3 \approx n^{1/2} \sum N_k r_k^3$. Using results from M. LaBarbera [*Science* **249**, 992 (1990)], who used data averaged over the first 160 vessels (approximately the first 4 levels), gives, for human beings, $A_0 \approx 4.90 \text{ cm}^2$, $\bar{A}_K \approx 19.98 \text{ cm}^2$, $r_0^3 \approx 1.95 \text{ cm}^3$, and $\sum N_k r_k^3 \approx 1.27 \text{ cm}^3$, in agreement with area preservation. LaBarbera, unfortunately, took the fact that $\bar{A}_K \neq A_0$ and $r_0^3 \approx \sum N_k r_k^3$ as evidence for cubic rather than area-preserving branching. For small vessels, where $k > k$, convincing evidence for the cubic law can be found in the analysis of the arteriolar system by M. L. Ellsworth *et al.*, *Microvasc. Res.* **34**, 168 (1987).

21. Y. C. Fung, *Biodynamics* (Springer-Verlag, New York, 1984).
22. P. Gehr *et al.*, *Respir. Physiol.* **44**, 61 (1981).
23. P. M. Bennett and P. H. Harvey, *J. Zool.* **213**, 327 (1987); A. F. Bennett, *Am. Zool.* **28**, 699 (1988); P. H. Harvey and M. D. Pagel, *The Comparative Method in Evolutionary Biology* (Oxford Univ. Press, Oxford, 1991).
24. This is reminiscent of the invariance of scaling exponents to details of the model that follow from renormalization group analyses, which can be viewed as a generalization of classical dimensional analysis.
25. J.H.B. is supported by NSF grant DEB-9318096, B.J.E. by NSF grant GER-9553623 and a Fulbright Fellowship, and G.B.W. by the Department of Energy.

13 September 1996; accepted 12 February 1997

Flexibility in DNA Recombination: Structure of the Lambda Integrase Catalytic Core

Hyock Joo Kwon, Radhakrishna Tirumalai, Arthur Landy,*
Tom Ellenberger*

Lambda integrase is archetypic of site-specific recombinases that catalyze intermolecular DNA rearrangements without energetic input. DNA cleavage, strand exchange, and religation steps are linked by a covalent phosphotyrosine intermediate in which Tyr³⁴² is attached to the 3'-phosphate of the DNA cut site. The 1.9 angstrom crystal structure of the integrase catalytic domain reveals a protein fold that is conserved in organisms ranging from archaeobacteria to yeast and that suggests a model for interaction with target DNA. The attacking Tyr³⁴² nucleophile is located on a flexible loop about 20 angstroms from a basic groove that contains all the other catalytically essential residues. This bipartite active site can account for several apparently paradoxical features of integrase family recombinases, including the capacity for both cis and trans cleavage of DNA.

The integrase protein (Int) of *Escherichia coli* phage lambda (λ) belongs to a large family of site-specific DNA recombinases from archaeobacteria, eubacteria, and yeast (1–3) that catalyze rearrangements be-

tween DNA sequences with little or no sequence homology to each other (4–8). Like λ Int, many of these recombinases function in the integration and excision of viral genomes into and out of the chromosomes of their respective hosts. Others function in the decatenation or segregation of newly replicated chromosomes, conjugative transposition, regulation of plasmid copy number, or expression of cell surface proteins. Integrase family members have the distinctive ability to carry out a complete site-specific recombination reac-

H. J. Kwon and T. Ellenberger, Department of Biological Chemistry and Molecular Pharmacology, Harvard Medical School, Boston MA 02115, and the Graduate Program in Biophysics, Harvard University, Cambridge, MA 02138, USA.

R. Tirumalai and A. Landy, Division of Biology and Medicine, Brown University, Providence, RI 02912, USA.

*Corresponding authors.